Proceedings of the ASME 2015 International Design Engineering Technical Conferences & Computers and Information in Engineering Conference
IDETC/CIE 2015
August 2-5, 2015, Boston, Massachusetts, USA

DETC2015-47037

THE EFFECT OF NON-SYMMETRIC FRF ON MACHINING: A CASE STUDY

David Hajdu
Department of Applied Mechanics
Budapest University of Technology and Economics
Budapest, Hungary
Email: hajdu@mm.bme.hu

Tamas Insperger
Department of Applied Mechanics
Budapest University of Technology and Economics
Budapest, Hungary
Email: insperger@mm.bme.hu

Gabor Stepan
Department of Applied Mechanics
Budapest University of Technology and Economics
Budapest, Hungary
Email: stepan@mm.bme.hu

ABSTRACT

Stability prediction of machining operations is often not reliable due to the inaccurate mechanical modeling. A major source of this inaccuracy is the uncertainties in the dynamic parameters of the machining center at different spindle speeds. The so-called tip-to-tip measurement is the fastest and most convenient method to determine the frequency response of the machine. This concept consists of the measurement of the tool tip's frequency response function (FRF) usually in two perpendicular directions including cross terms. Although the cross FRFs are often neglected in practical applications, they may affect the system's dynamics. In this paper, the stability diagrams are analyzed for milling operations in case of diagonal, symmetric and non-symmetric FRF matrices. First a time-domain model is derived by fitting a multiple-degrees-of-freedom model to the FRF matrix, then the semi-discretization method is used to determine stability diagrams. The results show that the omission of the non-symmetry of the FRF matrix may lead to inaccurate stability diagram.

1 INTRODUCTION

The maximum capabilities of machine tool centers are often not utilized due to limitations caused by machine tool chatter. Although in many applications very high cutting speeds are achievable, the arising harmful vibrations significantly limit the material removal rate. The prediction of the stability of the machining operation with high accuracy is therefore an important task.

In the 1960s, after the extensive work of Tobias [1] and Tlusty [2], the so-called regenerative effect became the most commonly accepted explanation for machine tool chatter. The phenomenon can be described by involving time delay in the model equations. The vibrations of the tool are copied onto the surface of the workpiece, which modifies the chip thickness and induces variation in the cutting-force acting on the tool one revolution later. This phenomenon can be described by delay-differential equations (DDEs).

Stability properties of the machining processes are depicted by the so-called stability lobe diagrams, which plot the maximum stable depths of cut versus the spindle speed. These diagrams provide a guide to the machinist to select the optimal technological parameters in order to achieve maximum material removal rate without chatter.

There exist several numerical techniques to predict the stability of machining operations. Some of them apply the measured frequency response functions (FRFs) directly, such as the single frequency solution, the multi-frequency solution [3, 4], the extended multi-frequency solution [5]. Other techniques, such as the semi-discretization method [6, 7], full-discretization method [8], Chebyshev collocation method [9, 10], spectral element method [11], the implicit subspace iteration method [12] or the integration method [13], require fitted modal parameters as input.

There are several limitations in the modeling of machine tool chatter. Most models in the literature consider linear systems, although nonlinear effects may also influence the stability

properties [14]. The number of modes to be modeled is also an important factor [15], and the approximation of the measured frequency response function (FRF) plays an important role [13], too.

The modal parameters of the system can be extracted from the measured FRFs using modal parameter estimation techniques. Methods, which are based on the fitting of measured FRFs, are called frequency-domain estimators, such as the Rational Fraction Polynomial method (RFP) [16], (Linear on Nonlinear) Least Squares Frequency-Domain algorithm (LSFD), Polyreference Least Squares Complex Frequency-domain estimator, Frequency-domain Direct Parameter Identification (FDPI) method or Frequency-domain Maximum Likelihood Estimator (MLE), just to mention a few. There also exist techniques using the impulse response function of the system in time domain, for instance the Ibrahim Time-Domain (ITD) method, Eigensystem Realization Algorithm (ERA), Least Squares Complex Exponential (LSCE) algorithm or other methods (see [17] and the references therein).

The fitted modal parameters are obtained from measurements, which are loaded by noise, parameter identification is therefore not a straightforward task. Besides the number of modes to be involved in the fitting, the properties of the mechanical model used for the fitting (e.g., proportional vs. non-proportional damping, symmetric vs. non-symmetric FRF matrix) also strongly affect the results.

In this paper, the sensitivity of the stability charts of milling operations with respect to the estimation of the cross FRFs is analyzed. The modal parameters are approximated using a frequency-domain nonlinear least squares method. Stability diagrams are then constructed using the semi-discretization method. It is shown that the omission of the non-symmetry of the FRF matrix may lead to inaccurate stability charts.

2 DETERMINATION OF MODAL PARAMETERS

The modal behavior of the machine is usually determined by means of impact or shaking tests [18]. The measured FRF contains information about the dynamics of the structure, from which the modal parameters can be extracted. Consider a matrix differential equation of motion for a multiple-degrees-of-freedom system in the form

$$\mathbf{M}\ddot{\mathbf{r}}(t)+\mathbf{C}\dot{\mathbf{r}}(t)+\mathbf{K}\mathbf{r}(t)=\mathbf{f}(t), \tag{1}$$

where $\mathbf{r}(t)\in\mathbb{R}^n$ is the generalized coordinate vector, $\mathbf{M}\in\mathbb{R}^{n\times n}$ is the mass matrix, $\mathbf{C}\in\mathbb{R}^{n\times n}$ is the damping matrix, $\mathbf{K}\in\mathbb{R}^{n\times n}$ is the stiffness matrix, $\mathbf{f}(t)\in\mathbb{R}^n$ is the excitation vector and n is the number of degrees of freedom. Matrices $\mathbf{M}$, $\mathbf{C}$, and $\mathbf{K}$ depend on the choice of the general coordinates, for which the underlying lumped model is often ambiguous. Therefore, for general cases, the equations of motion are usually defined in the modal space. In this section, three modeling concepts are described: (1) proportional damping; (2) non-proportional damping; and (3) non-symmetric FRF matrices.

2.1 Proportional damping

The system is proportionally damped if the damping matrix can be written as

$$\mathbf{C}=\alpha_{\mathrm{M}}\mathbf{M}+\alpha_{\mathrm{K}}\mathbf{K}, \tag{2}$$

where $\alpha_{\mathrm{M}}\in\mathbb{R}$ and $\alpha_{\mathrm{K}}\in\mathbb{R}$ are the proportional factors [19]. If the damping matrix can be written in this form, then it guarantees that the mode shapes are real valued and identical to the eigenvectors of the undamped system. The corresponding eigenvalue-eigenvector problem is formulated as

$$(\lambda^2\mathbf{M}+\mathbf{K})\mathbf{P}=\mathbf{0}, \tag{3}$$

where $\mathbf{P}_k\in\mathbb{R}^n$ $(k=1,2,\dots n)$ is the normal mode of the undamped system, $\lambda_k=\pm\mathrm{i}\omega_{\mathrm{n},k}$ with $\omega_{\mathrm{n},k}$ being the natural angular frequency of the undamped system and i is the imaginary unit. The mass-orthonormal eigenvectors can be defined as

$$\boldsymbol{\phi}_k=\frac{\mathbf{P}_k}{\sqrt{\mathbf{P}_k^{\mathrm{T}}\mathbf{M}\mathbf{P}_k}}, \tag{4}$$

and the modal transformation matrix $\boldsymbol{\Phi}$ can be given as

$$\boldsymbol{\Phi}=\begin{pmatrix}\boldsymbol{\phi}_1 & \boldsymbol{\phi}_2 & \cdots & \boldsymbol{\phi}_n\end{pmatrix}. \tag{5}$$

Using the modal transformation $\mathbf{r}(t)=\boldsymbol{\Phi}\mathbf{q}(t)$, Eq. (1) can be transformed into the n-dimensional modal space of the modal coordinates $\mathbf{q}(t)$, i.e.

$$\ddot{\mathbf{q}}(t)+[2\zeta_k\omega_{\mathrm{n},k}]\dot{\mathbf{q}}(t)+[\omega_{\mathrm{n},k}^2]\mathbf{q}(t)=\boldsymbol{\Phi}^{\mathrm{T}}\mathbf{f}(t). \tag{6}$$

The FRF matrix $\mathbf{H}(\omega)$ can be formulated as

$$\mathrm{H}_{ij}(\omega)=\frac{R_i(\omega)}{F_j(\omega)}=\sum_{k=1}^{n}\frac{\phi_{ik}\phi_{jk}}{-\omega^2+2\zeta_k\omega_{\mathrm{n},k}\omega\mathrm{i}+\omega_{\mathrm{n},k}^2}, \tag{7}$$

where ij represents the rows and columns of matrix $\mathbf{H}(\omega)$ respectively, $R_i(\omega)=\mathscr{F}(r_i(t))$, $F_i(\omega)=\mathscr{F}(f_i(t))$ with $\mathscr{F}$ denoting the Fourier transform and ζ_k is the damping ratio of the k^{th} mode. Note that $\mathbf{H}(\omega)=\mathbf{H}^{\mathrm{T}}(\omega)$. During a fitting process, four real parameters should be determined to each degree of freedom, namely, $\omega_{\mathrm{n},k}$, ζ_k, ϕ_{ik} and ϕ_{jk}, where $k=1,2\dots n$.

2.2 Non-proportional damping

A system is called non-proportionally damped if Eq. (2) does not hold. In this case, the FRFs cannot be expressed according to (7), furthermore the mode shapes are complex and they are not identical to the eigenvectors of the undamped system. The equation of motion can be written in a first-order form

$$\hat{\mathbf{A}}\dot{\mathbf{v}}(t)+\hat{\mathbf{B}}\mathbf{v}(t)=\mathbf{f}_{\mathbf{v}}(t), \tag{8}$$

where the state vector is $\mathbf{v}(t)=(\mathbf{r}^{\mathrm{T}}(t)\ \dot{\mathbf{r}}^{\mathrm{T}}(t))^{\mathrm{T}}$ and

$$\hat{\mathbf{A}}=\begin{pmatrix}\mathbf{C} & \mathbf{M}\\ \mathbf{M} & \mathbf{0}\end{pmatrix},\quad \hat{\mathbf{B}}=\begin{pmatrix}\mathbf{K} & \mathbf{0}\\ \mathbf{0} & -\mathbf{M}\end{pmatrix},\quad \mathbf{f}_{\mathbf{v}}(t)=\begin{pmatrix}\mathbf{f}(t)\\ \mathbf{0}\end{pmatrix}, \tag{9}$$

furthermore $\hat{\mathbf{A}}=\hat{\mathbf{A}}^{\mathrm{T}}$ and $\hat{\mathbf{B}}=\hat{\mathbf{B}}^{\mathrm{T}}$ [19, 20]. The eigenvalue-eigenvector problem associated with the homogeneous part of Eq. (8) reads

$$(\hat{\mathbf{A}}\lambda+\hat{\mathbf{B}})\mathbf{U}=\mathbf{0}, \tag{10}$$

where $\mathbf{U}\in\mathbb{C}^{2n}$ is the unnormalized (right) eigenvector. The eigenvalues can be determined from the frequency equation

$$\det(\hat{\mathbf{A}}\lambda+\hat{\mathbf{B}})=0, \tag{11}$$

where $\lambda_k=-\zeta_k\omega_{\mathrm{n},k}\pm\mathrm{i}\omega_{\mathrm{n},k}\sqrt{1-\zeta_k^2}$. The eigenvalues and eigenvectors form complex conjugate pairs if $\zeta_k<1$.

Equation (8) can be transformed into the $2n$-dimensional modal space by the transformation $\mathbf{v}(t)=\mathbf{\Psi}\mathbf{q}_{\mathbf{v}}(t)$, where $\mathbf{q}_{\mathbf{v}}(t)\in\mathbb{C}^{2n}$ is the modal coordinate vector and $\mathbf{\Psi}\in\mathbb{C}^{2n\times 2n}$ is the modal transformation matrix. Using the normalized eigenvectors

$$\boldsymbol{\psi}_k=\frac{\mathbf{U}_k}{\sqrt{\mathbf{U}_k^{\mathrm{T}}\hat{\mathbf{A}}\mathbf{U}_k}}, \tag{12}$$

the modal transformation matrix can be written as

$$\mathbf{\Psi}=\begin{pmatrix}\boldsymbol{\psi}_1 & \bar{\boldsymbol{\psi}}_1 & \cdots & \boldsymbol{\psi}_n & \bar{\boldsymbol{\psi}}_n\end{pmatrix}. \tag{13}$$

Since $\mathbf{\Psi}^{\mathrm{T}}\hat{\mathbf{A}}\mathbf{\Psi}=\mathbf{I}$ and

$$\mathbf{\Psi}^{\mathrm{T}}\hat{\mathbf{B}}\mathbf{\Psi}=-\begin{pmatrix}\ddots & & \\ & \lambda_k & 0\\ & 0 & \bar{\lambda}_k\\ & & \ddots\end{pmatrix}:=-\mathbf{\Lambda}, \tag{14}$$

the equations of motion finally can be given in the form

$$\dot{\mathbf{q}}_{\mathbf{v}}(t)-\mathbf{\Lambda}\mathbf{q}_{\mathbf{v}}(t)=\mathbf{\Psi}^{\mathrm{T}}\mathbf{f}_{\mathbf{v}}(t). \tag{15}$$

From the Fourier transform of Eq. (15), the elements of the FRF matrix $\mathbf{H}(\omega)$ can be formulated as

$$\mathrm{H}_{ij}(\omega)=\frac{R_i(\omega)}{F_j(\omega)}=\sum_{k=1}^{n}\left(\frac{\psi_{ik}\psi_{jk}}{\omega\mathrm{i}-\lambda_k}+\frac{\bar{\psi}_{ik}\bar{\psi}_{jk}}{\omega\mathrm{i}-\bar{\lambda}_k}\right). \tag{16}$$

Note that $\mathbf{H}(\omega)=\mathbf{H}^{\mathrm{T}}(\omega)$. Equations (16) and (7) are identical if the damping is proportional, in this case, $\mathrm{Re}\{\psi_{ik}\psi_{jk}\}=0$. Using curve-fitting techniques, the modal parameters $\omega_{\mathrm{n},k}$, ζ_k, ψ_{ik} and ψ_{jk}, where $k=1,2,\ldots n$ can be fitted on the measured FRF. Since ψ is complex, this gives 6 real parameters for each degree of freedom.

2.3 Non-symmetric FRF matrices

Engineering structures are often affected by additional forces, such as gyroscopic forces, rotor-stator rub forces, electromagnetic forces, unsteady aerodynamic forces or time-varying fluid forces [19]. As a result, any of these phenomena can destroy the symmetry of the system matrices and the previously presented modal formulations do not apply.

From the mathematical point of view, this problem can be treated in some cases [19, 21]. The mode shapes are generally complex, and the equation of motion is considered in the form (8), where $\hat{\mathbf{A}}\neq\hat{\mathbf{A}}^{\mathrm{T}}$ and $\hat{\mathbf{B}}\neq\hat{\mathbf{B}}^{\mathrm{T}}$ can both be non-symmetric. The diagonal transformation can be performed if the left and right eigenvectors of the system are calculated as

$$(\hat{\mathbf{A}}\lambda+\hat{\mathbf{B}})\mathbf{U}_{\mathrm{R}}=\mathbf{0}\quad\text{and}\quad(\hat{\mathbf{A}}^{\mathrm{T}}\lambda+\hat{\mathbf{B}}^{\mathrm{T}})\mathbf{U}_{\mathrm{L}}=\mathbf{0}, \tag{17}$$

where $\mathbf{U}_{\mathrm{R}}$ and $\mathbf{U}_{\mathrm{L}}$ are the unnormalized right and left eigenvectors respectively. According to [19], the right eigenvectors represent the mode shapes themselves while the left ones are associated with preferred excitation patterns.

The modal transformation matrices has to be normalized according to the criterion

$$\mathbf{\Psi}_{\mathrm{R}}=\frac{\mathbf{U}_{\mathrm{R}}}{\sqrt{\mathbf{U}_{\mathrm{L}}^{\mathrm{T}}\hat{\mathbf{A}}\mathbf{U}_{\mathrm{R}}}}\quad\text{and}\quad\mathbf{\Psi}_{\mathrm{L}}=\frac{\mathbf{U}_{\mathrm{L}}}{\sqrt{\mathbf{U}_{\mathrm{R}}^{\mathrm{T}}\hat{\mathbf{A}}^{\mathrm{T}}\mathbf{U}_{\mathrm{L}}}}, \tag{18}$$

therefore the normalized eigenvectors satisfy the properties $\mathbf{\Psi}_{\mathrm{L}}^{\mathrm{T}}\hat{\mathbf{A}}\mathbf{\Psi}_{\mathrm{R}}=\mathbf{I}$ and $\mathbf{\Psi}_{\mathrm{L}}^{\mathrm{T}}\hat{\mathbf{B}}\mathbf{\Psi}_{\mathrm{R}}=-\mathbf{\Lambda}$. Using the modal transformation $\mathbf{v}(t)=\mathbf{\Psi}_{\mathrm{R}}\mathbf{q}_{\mathbf{v}}(t)$, Eq. (8) can be written as

$$\dot{\mathbf{q}}_{\mathbf{v}}(t)-\mathbf{\Lambda}\mathbf{q}_{\mathbf{v}}(t)=\mathbf{\Psi}_{\mathrm{L}}^{\mathrm{T}}\mathbf{f}_{\mathbf{v}}(t). \tag{19}$$

The parametric expression for the elements of the frequency response function is

$$\mathrm{H}_{ij}(\omega) = \frac{R_i(\omega)}{F_j(\omega)} = \sum_{k=1}^{n} \left(\frac{\psi_{ik}^{\mathrm{R}} \psi_{jk}^{\mathrm{L}}}{\omega \mathrm{i} - \lambda_k} + \frac{\bar{\psi}_{ik}^{\mathrm{R}} \bar{\psi}_{jk}^{\mathrm{L}}}{\omega \mathrm{i} - \bar{\lambda}_k} \right). \tag{20}$$

It can be shown that $\mathrm{H}_{ij} \neq \mathrm{H}_{ji}$, i.e., the FRF matrix is not symmetric in this case. In practice, the measured cross FRFs are often close to each other, but sometimes significant differences can be observed, which can qualitatively affect the dynamical behavior of the system. If the cross FRFs are the same, then the system matrices are symmetric, the left and right eigenvectors are the same and $\mathbf{\Psi}_{\mathrm{R}} = \mathbf{\Psi}_{\mathrm{L}} = \mathbf{\Psi}$. Note, that during the fitting process, the measured non-symmetric cross frequency response functions have to be used. The unknown parameters are $\omega_{\mathrm{n},k}$, ζ_k, ψ_{ik}^{R}, ψ_{ik}^{L}, ψ_{jk}^{R}, ψ_{jk}^{L} and $k = 1,2 \ldots n$. Since ψ is complex, this results 10 real parameters for each degree of freedom.

3 MILLING OPERATION

The general equation of motion in case of multiple-degrees-of-freedom systems considering the typically intricate regeneration properties associated with a complex tool geometry reads [22]

$$\mathbf{M}\ddot{\mathbf{r}}(t) + \mathbf{C}\dot{\mathbf{r}}(t) + \mathbf{K}\mathbf{r}(t) = \mathbf{f}(t, \mathbf{r}_t(\vartheta)), \tag{21}$$

where $\mathbf{r}_t(\vartheta) = \mathbf{r}(t+\vartheta), \vartheta \in [-T, 0)$ and T is the occurring maximum delay, furthermore $\mathbf{f}(t, \mathbf{r}_t(\vartheta)) = (F_x \; F_y \; 0 \; \ldots \; 0)^{\mathrm{T}}$, where F_x and F_y are the cutting force components.

For convenience, a simple helical tool is assumed, with constant helix angle and equally distributed teeth. Tools with unequal tooth pitch and with varying helix angle are studied in [12,23] and in [20]. The helical tool analyzed here has N teeth of uniform helix angle β. According to [7], the tool is divided into elementary disks along the axial direction. The relation between the helix angle β and the helix pitch l_{p} is $\tan\beta = D\pi/(Nl_{\mathrm{p}})$, thus the angular position of the cutting edges along the axial direction reads

$$\varphi_j(t,z) = \frac{2\pi\Omega}{60} t + j\frac{2\pi}{N} - z\frac{2\pi}{Nl_{\mathrm{p}}}, \tag{22}$$

where z is the coordinate along the axial immersion. The elementary cutting-force components in tangential and radial directions acting on tooth j at a disk element of width $\mathrm{d}z$ are given as

$$\mathrm{d}F_{j,t}(t,z) = g_j(t,z) K_t h_j^q(t,z) \mathrm{d}z, \tag{23}$$

$$\mathrm{d}F_{j,r}(t,z) = g_j(t,z) K_r h_j^q(t,z) \mathrm{d}z, \tag{24}$$

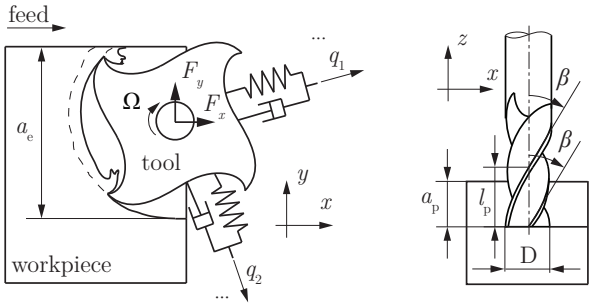

FIGURE 1. Dynamical model of milling operation.

where $h_j(t,z)$ is the chip thickness cut by the tooth j at axial immersion z. The screen function $g_j(t,z)$ reads

$$g_j(t,z) = \begin{cases} 1, & \text{if } \varphi_{\mathrm{en}} < (\varphi_j(t,z) \bmod 2\pi) < \varphi_{\mathrm{ex}}, \\ 0, & \text{otherwise.} \end{cases} \tag{25}$$

The actual chip thickness at tooth j can be calculated approximately as

$$\begin{aligned} h_j(t,z) \approx (f_{\mathrm{z}} + x(t-\tau) - x(t)) \sin\varphi_j(t,z) \\ + (y(t-\tau) - y(t)) \cos\varphi_j(t,z), \end{aligned} \tag{26}$$

where f_{z} is the feed per tooth, $x(t)$ and $y(t)$ are the displacements of the center of the tool, and $\tau = 60/(N\Omega)$ is the tooth-passing period. The components of the elementary cutting force acting on tooth j in direction x and y reads

$$\mathrm{d}F_{j,x}(t,z) = \mathrm{d}F_{j,t}(t,z)\cos\varphi_j(t,z) + \mathrm{d}F_{j,r}(t,z)\sin\varphi_j(t,z), \tag{27}$$

$$\mathrm{d}F_{j,y}(t,z) = -\mathrm{d}F_{j,t}(t,z)\sin\varphi_j(t,z) + \mathrm{d}F_{j,r}(t,z)\cos\varphi_j(t,z), \tag{28}$$

from which the resultant cutting forces can be calculated as

$$\begin{aligned} F_{j,x}(t) = \sum_{j=1}^{N} \int_0^{a_{\mathrm{p}}} \mathrm{d}F_{j,x}(t,z)\mathrm{d}z = \\ \sum_{j=1}^{N} \int_0^{a_{\mathrm{p}}} g_j(t,z)(K_t\cos\varphi_j(t,z) + K_r\sin\varphi_j(t,z)) h_j^q(t)\mathrm{d}z, \end{aligned} \tag{29}$$

$$\begin{aligned} F_{j,y}(t) = \sum_{j=1}^{N} \int_0^{a_{\mathrm{p}}} \mathrm{d}F_{j,y}(t,z)\mathrm{d}z = \\ \sum_{j=1}^{N} \int_0^{a_{\mathrm{p}}} g_j(t,z)(-K_t\sin\varphi_j(t,z) + K_r\cos\varphi_j(t,z)) h_j^q(t)\mathrm{d}z. \end{aligned} \tag{30}$$

Assuming small perturbation $\boldsymbol{\varepsilon}(t)$ around the periodic motion $\mathbf{r}_{\mathrm{p}}(t)$ of stationary cutting, i.e. $\mathbf{r}(t) = \mathbf{r}_{\mathrm{p}}(t) + \boldsymbol{\varepsilon}(t)$, the linearized

equation of motion considering the delayed terms can be given in the form

$$\mathbf{M}\ddot{\boldsymbol{\varepsilon}}(t)+\mathbf{C}\dot{\boldsymbol{\varepsilon}}(t)+\mathbf{K}\boldsymbol{\varepsilon}(t)=\boldsymbol{\kappa}(t)(\boldsymbol{\varepsilon}(t-\tau)-\boldsymbol{\varepsilon}(t)), \tag{31}$$

where the specific directional factor matrix $\boldsymbol{\kappa}(t)$ can be calculated as

$$\boldsymbol{\kappa}(t)=\frac{\partial \mathbf{f}(t,t-\tau)}{\partial \mathbf{r}(t-\tau)}=\begin{pmatrix} \kappa_{xx}(t) & \kappa_{xy}(t) & 0\cdots 0 \\ \kappa_{yx}(t) & \kappa_{yy}(t) & 0\cdots 0 \\ 0 & 0 & 0\cdots 0 \\ \vdots & \vdots & \vdots \quad \vdots \\ 0 & 0 & 0\cdots 0 \end{pmatrix}. \tag{32}$$

Note, that $\boldsymbol{\kappa}(t)=\boldsymbol{\kappa}(t+\tau)$ is also periodic. Since only the tool tip is forced, matrix $\boldsymbol{\kappa}(t)$ in the spatial *xyz* representation contains only four nonzero elements, which are

$$\kappa_{xx}(t)=\sum_{j=1}^{N} q f_z^{q-1}\int_0^{a_p}\big(g_j(t,z)\left(K_t\cos\varphi_j(t,z)+K_r\sin\varphi_j(t,z)\right) \sin^q\varphi_j(t,z)\big)\mathrm{d}z, \tag{33}$$

$$\kappa_{xy}(t)=\sum_{j=1}^{N} q f_z^{q-1}\int_0^{a_p}\big(g_j(t,z)\left(K_t\cos\varphi_j(t,z)+K_r\sin\varphi_j(t,z)\right) \cos\varphi_j(t,z)\sin^{q-1}\varphi_j(t,z)\big)\mathrm{d}z, \tag{34}$$

$$\kappa_{yx}(t)=\sum_{j=1}^{N} q f_z^{q-1}\int_0^{a_p}\big(g_j(t,z)\left(-K_t\sin\varphi_j(t,z)+K_r\cos\varphi_j(t,z)\right) \sin^q\varphi_j(t,z)\big)\mathrm{d}z, \tag{35}$$

$$\kappa_{yy}(t)=\sum_{j=1}^{N} q f_z^{q-1}\int_0^{a_p}\big(g_j(t,z)\left(-K_t\sin\varphi_j(t,z)+K_r\cos\varphi_j(t,z)\right) \cos\varphi_j(t,z)\sin^{q-1}\varphi_j(t,z)\big)\mathrm{d}z. \tag{36}$$

Since the system can be non-proportionally damped, the governing equation can be formulated as

$$\hat{\mathbf{A}}\dot{\mathbf{z}}(t)+\hat{\mathbf{B}}\mathbf{z}(t)=\tilde{\boldsymbol{\kappa}}(t)(\mathbf{z}(t-\tau)-\mathbf{z}(t)), \tag{37}$$

where the state vector is $\mathbf{z}(t)=(\boldsymbol{\varepsilon}^{\mathrm{T}}(t)\ \dot{\boldsymbol{\varepsilon}}^{\mathrm{T}}(t))^{\mathrm{T}}$ and

$$\tilde{\boldsymbol{\kappa}}(t)=\begin{pmatrix}\boldsymbol{\kappa}(t) & \mathbf{0}\\ \mathbf{0} & \mathbf{0}\end{pmatrix}. \tag{38}$$

Since the system matrices are non-symmetric, Eq. (37) can be transformed into the $2n$-dimensional modal space by the transformation $\mathbf{z}(t)=\boldsymbol{\Psi}_{\mathrm{R}}\mathbf{q}_{\mathbf{v}}(t)$. The governing equation is obtained as

$$\dot{\mathbf{q}}_{\mathbf{v}}(t)-\boldsymbol{\Lambda}\mathbf{q}_{\mathbf{v}}(t)=\boldsymbol{\Psi}_{\mathrm{L}}^{\mathrm{T}}\tilde{\boldsymbol{\kappa}}(t)\boldsymbol{\Psi}_{\mathrm{R}}(\mathbf{q}_{\mathbf{v}}(t-\tau)-\mathbf{q}_{\mathbf{v}}(t)). \tag{39}$$

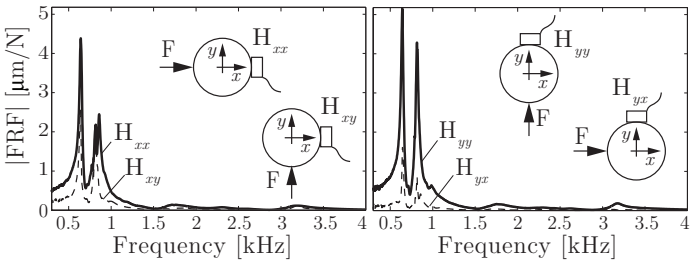

FIGURE 2. Measured frequency response functions (data taken from [18]).

The state space equations can be introduced in the form

$$\dot{\mathbf{q}}_{\mathbf{v}}(t)=\mathbf{A}(t)\mathbf{q}_{\mathbf{v}}(t)+\mathbf{B}(t)\mathbf{u}(t-\tau), \tag{40}$$

$$\mathbf{u}(t)=\mathbf{D}\mathbf{q}_{\mathbf{v}}(t), \tag{41}$$

where $\mathbf{A}(t)=\boldsymbol{\Lambda}-\boldsymbol{\Psi}_{\mathrm{L}}^{\mathrm{T}}\tilde{\boldsymbol{\kappa}}(t)\boldsymbol{\Psi}_{\mathrm{R}}$, $\mathbf{B}(t)=\boldsymbol{\Psi}_{\mathrm{L}}^{\mathrm{T}}\tilde{\boldsymbol{\kappa}}(t)$ and $\mathbf{D}=\boldsymbol{\Psi}_{\mathrm{R}}$. In case of a 2-dimensional tip-to-tip measurement, four FRFs can be evaluated and fitted. The state matrices in that case can be simplified to

$$\mathbf{A}(t)=\boldsymbol{\Lambda}-\boldsymbol{\Psi}_{\mathrm{L}}^{\mathrm{T}}\tilde{\boldsymbol{\kappa}}(t)\boldsymbol{\Psi}_{\mathrm{R}}, \tag{42}$$

$$\mathbf{B}(t)=\begin{pmatrix}\psi_{1i}^{\mathrm{L}} & \bar{\psi}_{1i}^{\mathrm{L}} & \cdots & \psi_{ni}^{\mathrm{L}} & \bar{\psi}_{ni}^{\mathrm{L}}\\ \psi_{1j}^{\mathrm{L}} & \bar{\psi}_{1j}^{\mathrm{L}} & \cdots & \psi_{nj}^{\mathrm{L}} & \bar{\psi}_{nj}^{\mathrm{L}}\end{pmatrix}^{\mathrm{T}}\begin{pmatrix}\kappa_{xx}(t) & \kappa_{xy}(t)\\ \kappa_{yx}(t) & \kappa_{yy}(t)\end{pmatrix}, \tag{43}$$

$$\mathbf{D}=\begin{pmatrix}\psi_{1i}^{\mathrm{R}} & \bar{\psi}_{1i}^{\mathrm{R}} & \cdots & \psi_{ni}^{\mathrm{R}} & \bar{\psi}_{ni}^{\mathrm{R}}\\ \psi_{1j}^{\mathrm{R}} & \bar{\psi}_{1j}^{\mathrm{R}} & \cdots & \psi_{nj}^{\mathrm{R}} & \bar{\psi}_{nj}^{\mathrm{R}}\end{pmatrix}. \tag{44}$$

In this paper, three different modeling concepts are investigated, all of them assume non-proportional damping. First, it is assumed that the vibrations in directions *x* and *y* are independent, i.e. the measured cross FRFs are neglected. This is an often used concept in the literature. Second, a symmetric FRF matrix is considered, where the vibration modes are not parallel to the directions *x* and *y*. Third, the effect of non-symmetric FRF matrix is analyzed. This phenomenon typically occurs in case of gyroscopic effect, magnetic field, nonlinearities or fluid-structure interaction [19]. Moreover, in real studies the measured structure usually shows some non-symmetry as a result of these or several other effects. In Fig. 2 a measured example can be seen (data taken from [18]), where H_{xy} means that the vibrations of the tool tip is measured in direction *x* but excited in direction *y*. As it can be seen, the cross FRFs (H_{xy} and H_{yx}) indicated by dashed lines cannot be neglected compared to the diagonal FRFs (H_{xx} and H_{yy}) indicated by solid line.

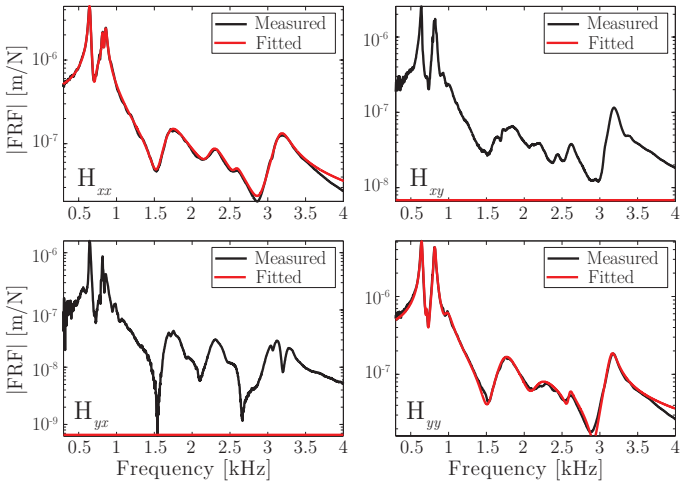

FIGURE 3. Fitted FRFs in case of diagonal FRF matrix, where the cross terms are neglected.

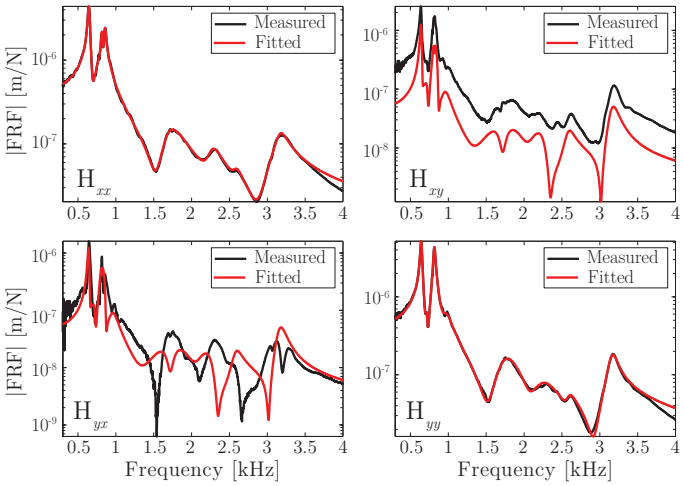

FIGURE 4. Fitted FRFs in case of symmetric FRF matrix, where the cross terms are the same.

4 STABILITY ANALYSIS

For periodic delay-differential equations, the Floquet theory applies. The solution segment of $\mathbf{w}_t$ for a general linear time-periodic DDE of the form

$$\dot{\mathbf{w}}(t) = \mathbf{L}(t, \mathbf{w}_t), \quad \mathbf{L}(t+T, .) = \mathbf{L}(t, .) \tag{45}$$

associated with the initial function $\mathbf{w}_0$ can be given as $\mathbf{w}_t = \mathscr{U}(t)\mathbf{w}_0$, where $\mathbf{w}_t(\vartheta) = \mathbf{w}(t+\vartheta)$, $\vartheta \in [-\tau, 0)$, $\mathbf{L}$ is a a linear functional, which is periodic in its first argument, furthermore T is the principal period and $\mathscr{U}(t)$ is the infinite-dimensional solution operator. The stability of the system is determined by the spectrum of the corresponding monodromy operator $\mathscr{M} = \mathscr{U}(T)$ [7]. This operator usually cannot be determined in closed form but can be approximated numerically.

Based on the semi-discretization method [7], the periodic coefficients are approximated by piece-wise constant terms, i.e.

$$\mathbf{A}_k = \frac{1}{h}\int_{t_k}^{t_{k+1}} \mathbf{A}(t)\mathrm{d}t, \qquad \mathbf{B}_k = \frac{1}{h}\int_{t_k}^{t_{k+1}} \mathbf{B}(t)\mathrm{d}t \tag{46}$$

where $k = 1, 2 \ldots p$, $\tau = ph$ and p is the number of the discretization steps over the principal period. Based on the analytical solution of Eqs. (40)-(41) assuming piecewise constant coefficient matrices, the linear mapping which projects the solution to the next time step can be formulated as

$$\mathbf{Q}_{k+1} = \mathbf{G}_k \mathbf{Q}_k, \tag{47}$$

where $\mathbf{Q}_k = (\mathbf{q}_{\mathbf{v},k}^{\mathrm{T}}\ \mathbf{u}_{k-1}^{\mathrm{T}}\ \cdots\ \mathbf{u}_{k-p}^{\mathrm{T}})^{\mathrm{T}}$. Finally, the monodromy operator is approximated by the transition matrix $\mathbf{\Pi}$ as

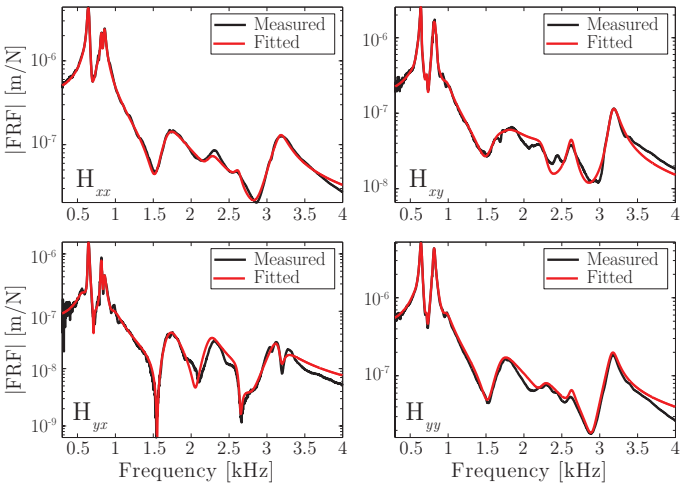

FIGURE 5. Fitted FRFs in case of non-symmetric FRF matrix, where the cross terms are different.

$$\mathbf{Q}_{k+p} = \mathbf{\Pi}\mathbf{Q}_k = \mathbf{G}_{k+p-1}\mathbf{G}_{k+p-2}\cdots\mathbf{G}_k\mathbf{Q}_k, \tag{48}$$

which is a finite-dimensional discrete approximation of the monodromy operator. The eigenvalues are calculated from the characteristic equation $\det(\mu\mathbf{I} - \mathbf{\Pi}) = 0$. The system is stable if all the complex eigenvalues μ_k are located inside the unit circle of the complex plane.

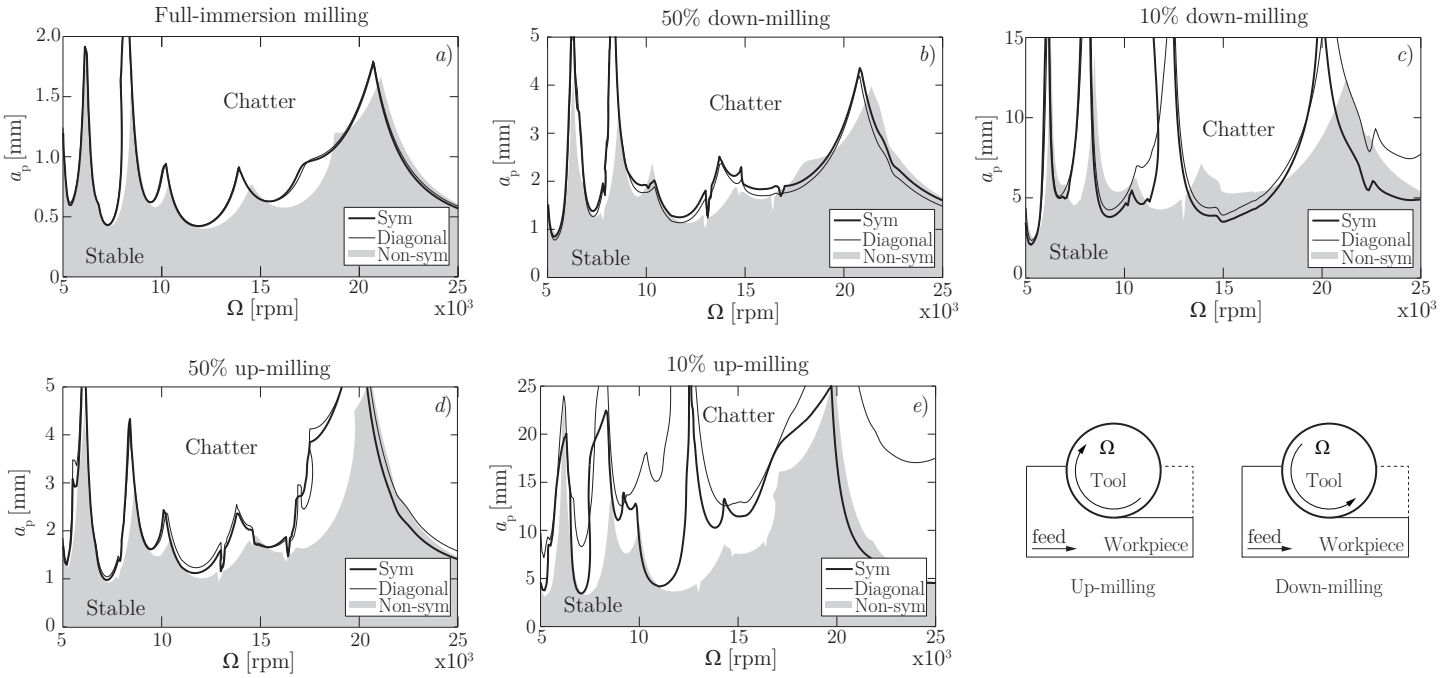

FIGURE 6. Stability charts for different milling operations and radial immersion.

5 A CASE STUDY

The measured FRFs is shown in Fig. 2. It can be seen that the cross functions (denoted by dashed lines) are in the magnitude of the diagonal FRFs, therefore they cannot be neglected. The parameters of the analyzed machining process are $q = 1$, $K_t = 500 \cdot 10^6$ N/m^2, $K_r = 200 \cdot 10^6$ N/m^2 and $f_z = 0.05$ mm/tooth, while a simple two-fluted tool with constant helix angle $\beta = 45^\circ$ and diameter $D = 20$ mm was assumed.

5.1 Fitted FRFs

Different fitted FRFs were determined using the theories presented previously. First, it is assumed that the cross FRFs can be neglected and the diagonal functions are fitted independently using two 8-degrees-of-freedom models in the x- and y-directions (referred as 'Diagonal FRFs'). The corresponding FRFs can be seen in Fig. 3. Note, that the scale is logarithmic in order to make visible the least dominant modes too, which are the most difficult to fit.

Second, the symmetric formulation was used (referred as 'Sym. cross FRFs'). In this case, all of the four measured functions are fitted simultaneously. The fitted functions of a 16-degrees-of-freedom model can be seen in Fig. 4. Since the cross terms are significantly different, the fitted cross function cannot approximate any of the them properly.

Third, the non-symmetry of the FRFs was also modeled. The fitted results are shown in Fig. 5. Again, a 16-degrees-of-freedom model was used during the fitting. Note, that the fitted diagonal FRFs are almost the same for all the three fitting concepts.

5.2 Sensitivity of stability charts

Once the measured FRFs are fitted, the semi-discretization method can be used. The stability charts of the different models can be seen in Fig. 6 for 10% and 50% radial immersion down-milling (i.e., $a_e/D = 0.1$ and 0.5), for full-immersion milling (i.e., $a_e/D = 1$), and for 10% and 50% radial immersion up-milling. The sketch of down-milling and up-milling can also be seen in Fig. 6. Solid thin line represents the boundary of the stable domain in case of a diagonal FRF matrix, solid thick line in case of symmetric FRF matrix, while grey shaded area corresponds to the stable domains obtained in case of non-symmetric FRF matrix. All results were checked by the extended multi-frequency solution introduced in [5], which showed good agreement with the results obtained by the semi-discretization method.

Stability diagram for full-immersion milling operation can be seen in panel a). The difference between stability boundaries obtained by the different concepts is not significant. The diagonal and symmetric FRF provides practically the same stability chart, while the non-symmetric case slightly differs. Note, that the difference increases as the spindle speed increases, i.e., the chart is sensitive at higher speeds.

The 50% down-milling operation in panel b) is more sensitive to the estimation of the cross FRFs, however the diagonal and symmetric FRF matrices provide almost the same stability

boundaries similarly to the full-immersion case. The 10% down-milling process presented in panel c) shows significant difference between the different models.

The results for the up-milling processes are similar. In case of a 50% up-milling operation, which is presented in panel d), the symmetric and the diagonal FRFs provide similar stability boundaries, but the boundaries corresponding to the non-symmetric model is clearly different especially for higher spindle speeds. In panel e), a 10% up-milling process is studied. It shows surprisingly large sensitivity, all of the three different models give very different results.

CONCLUSION

Prediction of the stability of a machining operation requires information about the modal behavior of the machining center. The frequency response functions can only be determined by experiments, which is usually noisy and may involve several uncertain factors. In this aspect, modal fitting can be considered as a filter: only the significant modes are used, which can clearly be distinguished form noise. However, if some modes are not identified properly, then the resulted stability diagrams may not reflect the properties of the real structure. On the other hand, if a frequency-domain method is used for stability prediction (e.g., multi-frequency solution), which uses directly the measured FRFs without any filtering, then the uncertainties of the measurements are transferred to the stability boundaries.

The most convenient measurement technique is the measurement of the tool tip. The modal response of the tool is measured and excited in two perpendicular directions. This results two diagonal FRFs and two cross FRFs. The cross FRFs are usually neglected and only the diagonal functions are fitted. Although the fitting process is simpler in this case, the resulted stability boundaries can be significantly different. In this work, the effect of the estimation of the cross FRFs is studied for milling operations.

The case study shows that the inaccurate approximation of the cross frequency response function can significantly affect the stability diagram, moreover the sensitivity is generally larger for processes with small radial immersions. It has to be highlighted that the stability properties are sensitive to the non-symmetry of the FRF matrix, which is an important issue from the operational point of view. At high speeds, for instance, the gyroscopic effect of the rotating elements of the spindle can be significant, and the operational modal behavior and the corresponding stability charts can be substantially different. If the gyroscopic effect cannot be neglected, then even if the measured static structure has symmetric FRFs, during the operation the symmetry fails and the stability chart changes.

ACKNOWLEDGMENT

This work was supported by the Hungarian National Science Foundation under grant OTKA-K105433. The research leading to these results has received funding from the European Research Council under the European Unions Seventh Framework Programme (FP/2007-2013) / ERC Advanced Grant Agreement n. 340889.

REFERENCES

[1] Tobias, S., 1965. *Machine-tool Vibration*. Blackie, Glasgow.

[2] Tlusty, J., and Spacek, L., 1954. *Self-excited vibrations on machine tools*. Nakl. CSAV, Prague. in Czech.

[3] Altintas, Y., and Budak, E., 1995. "Analytical prediction of stability lobes in milling". *CIRP AnnManuf Techn,* ***44***, pp. 357–362.

[4] Budak, E., and Altintas, Y., 1998. "Analytical prediction of chatter stability in milling, part i: General formulation". *J Dyn SystT ASME,* ***120***, pp. 22–30.

[5] Bachrathy, D., and Stepan, G., 2013. "Improved prediction of stability lobes with extended multi frequency solution". *CIRP AnnManuf Techn,* ***62***, pp. 411–414.

[6] Insperger, T., and Stepan, G., 2002. "Semi-discretization method for delayed systems". *Int J Numer Meth Eng,* ***55***, pp. 503–518.

[7] Insperger, T., and Stepan, G., 2011. *Semi-discretization for time-delay systems*, Vol. 178. Springer, New York.

[8] Ding, Y., Zhu, L. M., Zhang, X. J., and Ding, H., 2010. "A full-discretization method for prediction of milling stability". *Int J Mach Tool Manu,* ***50***, p. 502509.

[9] Butcher, E. A., Bobrenkov, O. A., Bueler, E., and Nindujarla, P., 2009. "Analysis of milling stability by the chebyshev collocation method: algorithm and optimal stable immersion levels". *J Comput Nonlin DynT ASME,* ***4***, p. 031003.

[10] Totis, G., Albertelli, P., Sortino, M., and Monno, M., 2014. "Efficient evaluation of process stability in milling with spindle speed variation by using the chebyshev collocation method". *J Sound Vib,* ***333***, p. 646668.

[11] Khasawneh, F. A., and Mann, B. P., 2011. "A spectral element approach for the stability of delay systems". *Int J Numer Meth Eng,* ***87***, p. 566952.

[12] Zatarain, M., and Dombovari, Z., 2014. "Stability analysis of milling with irregular pitch tools by the implicit subspace iteration method". *Int J Dynam Control,* ***2***, pp. 26–34.

[13] Zhang, X. J., Xiong, C. H., Ding, Y., Feng, M. J., and Xiong, Y. L., 2012. "Milling stability analysis with simultaneously considering the structural mode coupling effect and regenarative effect". *Int J Mach Tool Manu,* ***53***, pp. 127–140.

[14] Dombovari, Z., Wilson, R. E., and Stepan, G., 2008. "Es-

timates of the bistable region in metal cutting". *P Roy Soc AMath Phy,* ***464***, pp. 3255–3271.
[15] Munoa, J., Dombovari, Z., Mancisidor, I., Yang, Y., and Zatarain, M., 2013. "Interaction between multiple modes in milling processes". *Mach Sci Technol,* ***17***, pp. 165–180.
[16] Richardson, M. H., and Formenti, D. L., 1982. "Parameter estimation from frequency response measurement using rational fraction polinomials". In 1st IMAC Conference.
[17] Verboven, P., 2002. *Frequency-domain system identification for modal analysis, PhD Thesis*. Vrije Universiteit Brussel, Pleinlaan 2, B-1050 Brussels, Belgium.
[18] Dombovari, Z., and Stepan, G., 2011. "Marószerszámok dinamikai tulajdonságai és azok hatása a megmunkálás stabilitására". *GÉP.* in Hungarian.
[19] Ewins, D. J., 2000. *Modal Testing, Theory, Practice, and Application*. Research Studies Press 2nd edition.
[20] Dombovari, Z., Munoa, J., and Stepan, G., 2012. "General milling stability model for cylindrical tools". In 3rd CIRP Conference on Process Machine Interactions (3rd PMI), Elsevier, Procedia CIRP 4, pp. 90–97.
[21] Gutierrer-Wing, E. S., 2003. *Modal analysis of rotating machinery structures, PhD Thesis*. Imperial College London, University of London.
[22] Dombovari, Z., Iglesias, A., Zatarain, M., and Insperger, T., 2011. "Prediction of multiple dominant chatter frequencies in milling processes". *Int J Mach Tool Manu,* ***51***, pp. 457–464.
[23] Sellmeier, V., and Denkena, B., 2011. "Stable islands in the stability chart of milling processes due to unequal tooth pitch". *Int J Mach Tool Manu,* ***51***, pp. 152–164.